Ecotoxicology and Environmental Safety 293 (2025) 118007

Contents lists available at ScienceDirect

Ecotoxicology and Environmental Safety

journal homepage: www.elsevier.com/locate/ecoenv

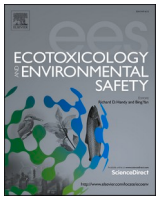

In vitro cell-transforming capacity of micro- and nanoplastics derived from 3D-printing waste

Adriana Rodríguez-Garraus [a], Mari Venäläinen [a], Jussi Lyyränen [a], Hanna Pulli [a], Apostolos Salmatonidis [b], Davide Lotti [c], Josefa Domenech [a], José F. Fernández [d], Jesús Guzmán-Mínguez [d,e], Mikel Isasi-Vicente [f], Alberto Katsumiti [f], Isabel Rodríguez-Llopis [f], Socorro Vázquez-Campos [b], Marie Carrière [g], Julia Catalán [a,h,*]

[a] *Finnish Institute of Occupational Health, Helsinki 00250, Finland*
[b] *LEITAT Technological Center, Terrassa 08225, Spain*
[c] *LATI Industria Termoplastici S.p.A., Vedano Olona 21040, Italy*
[d] *Instituto de Cerámica y Vidrio, ICV-CSIC, Madrid 28049, Spain*
[e] *Univ. Antonio de Nebrija, Industrial Engineering Department, Campus de Madrid-Princesa, Madrid 28015, Spain*
[f] *GAIKER Technology Centre, Basque Research and Technology Alliance (BRTA), Zamudio 48170, Spain*
[g] *Univ. Grenoble-Alpes, CEA, CNRS,Grenoble-INP, IRIG, SyMMES-CIBEST, Grenoble 38000, France*
[h] *Department of Anatomy, Embryology and Genetics, University of Zaragoza, Zaragoza 50013, Spain*

ARTICLE INFO

Edited by Professor Bing Yan

Keywords:
Microplastics
Nanoplastics
3D printing waste
Cell transformation
Carcinogenicity
Gene expression

ABSTRACT

The increasing use of plastic polymers in 3D printing applications may lead to human exposure to micro- and nanoplastics (MNPLs), raising concerns regarding adverse health consequences such as cancer induction. Little attention has been given to MNPLs originated at the end of the life cycle of 3D-printed objects because of the mechanical and environmental degradation of plastic waste. This study assessed the carcinogenic potential of secondary MNPLs generated through cryomilling of 3D objects using the validated *in vitro* Bhas 42 cell transformation assay (CTA). Three-dimensional objects were printed using four types of polycarbonate (PC)- and polypropylene (PP)-modified thermoplastic filaments, undoped and doped with single-walled carbon nanotubes (PC-CNT) and silver nanoparticles (PP-Ag), respectively. MNPLs (< 5 μm) generated following a three-step top-down process were thoroughly characterized. Bhas 42 cells were treated once (initiation assay) or repeatedly (promotion assay) with several concentrations of MNPLs (3.125–100 μg/mL) mimicking realistic exposure conditions, and transformed foci formation was evaluated after 21 days. Furthermore, cellular internalization and the mRNA expression of seven genes previously recognized as part of a predictive early cell transformation signature were also evaluated. Despite being internalized, none of the particles was able to initiate or promote *in vitro* cell transformation, regardless of doping with nanomaterials. Alternatively, all the particles significantly increased and decreased the mRNA expression of *Prl2c3* and *Timp4*, respectively, under promotion conditions, indicating early changes that occur before the formation of transformed foci. These findings suggest that the test MNPLs could have a tumorigenic potential despite not showing morphological changes in Bhas 42 cells.

1. Introduction

Three-dimensional (3D) printing techniques are increasingly used to manufacture different components in a customized way in both occupational and home settings (Sola and Trinchi, 2023). Fused deposition modeling (FDM), which consists of extruding a thermoplastic filament in a series of layers onto a printing plate, is presently the most widespread 3D printing technique for multiple applications (Burkhardt et al., 2022; Sola and Trinchi, 2023). Polycarbonate (PC) is one of the most prominent engineering thermoplastics applied in FDM (Ligon et al., 2017). Alternatively, polyolefins such as polypropylene (PP), which is one of the most widely used plastic materials worldwide (Plastics Europe, 2023), represents a cost-effective alternative to produce medical devices via extrusion-based printing (Burkhardt et al., 2022; Zhang and Gao,

* Corresponding author at: Department of Anatomy, Embryology and Genetics, University of Zaragoza, Zaragoza 50013, Spain.
E-mail address: jcatalan@unizar.es (J. Catalán).

https://doi.org/10.1016/j.ecoenv.2025.118007
Received 21 November 2024; Received in revised form 7 February 2025; Accepted 3 March 2025
Available online 10 March 2025

2022). The polymeric matrix can be reinforced with nanomaterials that confer advanced characteristics to the printed objects (Crapnell et al., 2024). For example, single-walled carbon nanotubes (SWCNTs) enhance the electrical and mechanical properties of polymers (Ding et al., 2023; Dokuchaeva et al., 2023), or silver nanoparticles increase the antibacterial efficacy of 3D-printed medical devices (Tse et al., 2021).

In recent years, increasing evidence of the release of micro- and nanoplastics (MNPLs) and volatile organic compounds during 3D printing processes has raised concerns regarding the potential health effects that these emissions could induce (Alijagic et al., 2024; Stefaniak et al., 2022). Emissions of about 4.1×10^{10} to 2.2×10^{11} particles/m^3 per minute have been reported for extrusion 3D printers using thermoplastics and resins (Azimi et al., 2016; Stefaniak et al., 2019), which are thousands of orders of magnitude higher than the estimated average concentration of MNPLs in the air (~50 particles/m^3) (Murashov et al., 2021). Exposure to airborne MNPLs can elicit chronic inflammation, which could lead to asthma, allergies, cardiac diseases and even cancer (Prata, 2018). Consequently, guidance for adopting safety measurements during 3D printing has been published (NIOSH, 2020). However, much less attention has been given to the potential generation of MNPLs at the end of the life cycle of printed objects, because of the mechanical and environmental degradation of plastic waste. Although 3D printing technologies are regarded as more sustainable than other manufacturing methods, plastic waste generated from 3D-printed polymer parts is rarely recycled and usually ends up in landfills (Filamentive, 2023; Patti, 2024). In the UK, the estimated plastic waste generated by filament-based 3D printing was approximately 379,000 kg in 2022 (Filamentive, 2023). Alternatively, 353 million tons of plastic waste were generated worldwide in 2019, out of which 65 million tons were generated by China ("Global Plastics Outlook," 2022; "Plastic Pollution - Our World in Data," 2023). Of these latter, 5000 tons (0.008 %) were probably 3D printing waste (Zhu et al., 2021). Despite these amounts looking small compared to other plastic waste sources, the problem is not negligible as 3D printing applications are expected to increase in the coming years.

Insights into fragmentation and environmental degradation of 3D printing waste, which can lead to the generation of MNPLs, are limited. UV-induced fragmentation rates of 50–200 μm primary microplastic polyamide and thermoplastic polyurethane powders used in 3D printing into 5–10 μm MNPL fragments were 0.951 and 0.589 mg/g/year, respectively (Pfohl et al., 2022). The abrasion rate for 3D printed dogbones of PC was estimated of up to 309 g/h for human use abrasion and up to 3.07×10^2 g/y for environmental abrasion (Sipe et al., 2022). Consequently, it is difficult to estimate which concentrations of 3D printing waste-derived MNPLs could be found in the environment, and how much they contribute to human exposure. Recent studies have detected MNPLs in environmental water compartments in a range of 10^2 to 10^9 particles/mL (Peng et al., 2024), which would correspond to 14.13×10^{-7} to 14.13 mg/mL for 1–5 μm MNPLs of spherical shape and a density of 1 g/cm^3 (ISO 24187:2023). Contaminant MNPLs, dispersed through water or air transmission, undergo biomagnification along the food chain and enter the human body through dietary ingestion and air inhalation (Zhao and You, 2024). Human MNPL intake has recently been estimated to be 50 – 500 mg/person/day through ingestion, and about 0.3 – 2.8 million particles/person/day by inhalation (Zhao and You, 2024). The highest intake rates correspond to countries from East Asia. Hence, assuming a similar percentage of 3D printing plastic waste as previously reported for China (0.008 %), that would mean a 3D printing-originated MNPL intake of about 40 μg/person/day only by ingestion in these countries.

Despite existing concerns for human health owing to the increasing environmental MNPL pollution, knowledge on the toxicity of MNPL remains scarce. The few available studies have mainly focused on short-term effects and have assessed pristine plastic particles (mainly polystyrene, PS), whereas very little information exists on secondary MNPLs that can be found in the environment (Domenech et al., 2023). One of the most critical concerns is the potential of MNPLs to induce cancer, as suggested by recent *in vivo* (Chen et al., 2024; Kim et al., 2022; Yang et al., 2023a) and *in vitro* (Barguilla et al., 2022b, 2022a) studies with commercial PS MNPLs. Furthermore, coexposure to MNPLs and associated nanomaterials may result in synergistic effects (Domenech et al., 2024). Based on these findings, it could be hypothesized that other MNPLs, such as those derived from 3D printing waste, may be carcinogenic.

In contrast to expensive and ethically concerned carcinogenesis studies in rodents, validated *in vitro* cell transformation assays (CTAs), as the Bhas 42 CTA (OECD, 2017), represent alternative robust and reproducible methods for simulating the first stages of tumorigenesis (Chatterjee and Alfaro-Moreno, 2023; Colacci et al., 2023). The Bhas 42 CTA consists of two parallel initiation and promotion assays, which allow for distinguishing genotoxic and nongenotoxic tumorigenic substances, respectively. Besides, an early mRNA expression signature has been described in Bhas 42 cells as a potential early biomarker of cell transformation (Guichard et al., 2023; Kirsch et al., 2020). Furthermore, Bhas 42 CTA has been successfully applied for assessing MNPLs. True-to-life polyethylene terephthalate (PET) nanoplastics promoted transformation of Bhas 42 cells, whereas polylactic acid (PLA) particles – a biobased polymer increasingly used in 3D printing (Ligon et al., 2017) – did not show tumorigenic capacity (Domenech et al., 2024).

In the present study, our hypothesis that 3D-printing waste-derived MNPLs could exert carcinogenic effects was tested by assessing the *in vitro* cell-transforming and gene expression dysregulation potential of these MNPLs using the validated Bhas 42 assay, which also provides insights into the underlying mechanisms of action. The assessed MNPLs were generated through cryomilling 3D-printed objects from four distinct types of plastic fibers: polycarbonate and polypropylene undoped and doped with SWCNTs and silver nanoparticles, respectively. The broad range of tested concentrations mimicked realistic exposure conditions. To the best of our knowledge, this is the first study to assess the tumorigenic potential of MNPLs generated from 3D printing plastic waste.

2. Methods

2.1. Obtention of particles

Small 3D-printed objects were produced using FDM of thermoplastic filaments manufactured by the LATI3DLab division of LATI Industria Termoplastici S.p.A. (LATI3Dlab) as previously described (McLean et al., 2024). Four distinct types of objects were produced according to the type and technical function of the filaments used in the process: polycarbonate-modified thermoplastic filaments, pristine ones (PC) and doped with 0.40–0.45 wt% SWCNTs/kg (PC-CNT); and polypropylene-modified thermoplastic filaments, pristine ones (PP) and doped with 0.05–0.10 wt% silver nanoparticles/kg (PP-Ag). SWCNT had an outer diameter of 1.6 nm and were > 5 μm long, whereas Ag particles had a spheroidal diameter of 15 nm (McLean et al., 2024). The nozzle temperatures used during the printing processes were 245–270 °C, and 250–290 °C for PP- and PC-based filaments, respectively.

MNPLs were obtained following a three-step top-down process. First, 3D-printed objects were cryomilled to the microscale using a Laboratory Knife Mill PULVERISETTE 11 (FRITSCH GmbH, Idar-Oberstein, Germany) for 2 min at 3600 rpm. Then, microsized particles were subjected to a high-energy mechanical milling step in water for 45 min (3 x 15 min cycles) at 420 rpm to obtain < 50 μm particles. Finally, the resulting particles were sieved through a 5 μm mesh to obtain a < 5 μm particle fraction, which was considered toxicologically relevant because it corresponds to the size threshold for cellular uptake (Champion et al., 2008; Yang et al., 2023).

Stock suspensions of each particle type were obtained following the NanoGenoTox protocol (Jensen et al., 2011). In brief, 15.36 mg of each material were weighed into glass vials and pre-wetted with 30 μl of

ethanol. Then, a solution of 0.05 % w/v bovine serum albumin (BSA; Sigma–Aldrich, Steinheim, Germany) was added to each vial to obtain 6 mL of a final concentration of 2.56 mg/mL. Samples were sonicated for 16 min using a 400 W, 60 Hz Branson Sonifier 450D (Branson Ultrasonics Corp, USA). The vials were vortexed for 30 seconds immediately before exposure. Fresh suspensions in water containing 0.05 % w/v BSA were prepared on the day of each treatment.

2.2. Characterization of micro- and nanosized particles

2.2.1. Microscopic characterization

The size, shape and elemental composition of the particles were determined using transmission electron microscopy/ energy dispersive X-ray spectroscopy (TEM/EDX). A droplet of each sample suspension in Milli-Q water was placed onto a SiO-coated copper grid (3.05 mm Ø) and air-dried. Samples were analyzed using a Jeol JEM-1400 Flash transmission electron microscope (Jeol Ltd., Tokyo, Japan) with a Jeol Dry SD30GV EDX detector operated at 80 kV. Images were obtained using a Jeol EM-14661 Flash sCMOS camera (Jeol Ltd.). In addition, PC and PC-CNT samples were analyzed with a DXR3 Raman microscope (Thermo Fisher Scientific, Waltham, USA) using a laser wavelength of 785 nm to verify the presence of SWCNTs.

For each TEM sample, 120 particles were measured from random fields and assumed to follow lognormal size distribution (Hinds, 2012). To obtain information on the morphology and aspect ratio, each particle was fitted inside an ellipse, and its main axles (a, b) were measured using software tools of the TEM Center v. 1.7.20 software (Jeol Ltd.). Data were processed using the MS Excel spreadsheet program. Chemical composition of the individual particles based on the assessment of 15–20 spectra per material type was determined through EDX via TEM. The latter analyses were performed both from entire particles and at specific areas, and covered different particle sizes.

2.2.2. Elemental chemical analysis

PP and PP-Ag samples were taken in triplicate and combined for the analyses. Samples were weighed, and digested in an ultrapure concentrated 6:1 nitric acid (HNO3 70 %): hydrofluoric acid (HF 49 %) mixture in an analytical microwave (Multiwave 7000, Anton Paar GmbH, Graz, Austria) following a 10 min ramp to reach 230 °C, after which the temperature was maintained for 20 min at 250 °C. The concentrations of Ag in the acid digests were determined using inductively coupled plasma—mass spectrometry (ICP-MS, Agilent 8900 ICP-QQQ, Agilent Technologies Inc., Santa Clara, CA, US). Quantification was conducted through interpolation on a calibration line prepared from commercial standards of silver (Inorganic Ventures, VA, USA). The limits of detection (LOD) and quantification (LOQ) were 0.05 and 0.1 mg/kg, respectively.

2.2.3. Hydrodynamic particle behavior

Hydrodynamic particle size and surface charge were measured in 0.05 % BSA-water suspensions and in culture media (DMEM/F12) using a ZetaPALS analyzer (Brookhaven Instruments Corporation, Holtsville, NY, USA). The average particle size and polydispersity index (PDI) were determined using dynamic light scattering (DLS) according to ISO 22412:2017. In addition, the surface charge was determined by measuring the Z-potential. All measurements were conducted in triplicate, and the data were analyzed using BIC Particle Solutions v2.6 software (Brookhaven Instruments Corporation). Statistical comparisons among particle types and between dispersion media were done through a two-way analysis of variance (ANOVA).

2.3. Assessment of cell-transforming potential

Bhas-42 cells were obtained from the Japanese Collection of Research Bioresources (JCRB) Cell Bank (Osaka, Japan). Cell culture and CTAs were performed as previously described (Domenech et al., 2024) following the recommendations of the OECD Guidance Document (GD) 231 (OECD, 2017), according to the six-well formatting protocol.

All the particles were tested up to 100 μg/mL, as previously recommended by the European Food Safety Agency when performing *in vitro* testing of nano-sized materials (More et al., 2021). Lower concentrations were set up at 2-fold intervals to cover a range of concentrations (3.125–100 μg/mL) that can be considered realistic according to the exposure estimates reported at the Introduction (Section 1). In addition, 1 μg/mL 3-methylcholanthrene (MCA, Sigma—Aldrich, Darmstadt, Germany) and 0.05 μg/mL 12-O-tetra-decanoylphorbol 13-acetate (TPA, Sigma—Aldrich) were used as positive controls for the initiation and promotion assays, respectively. Caffeine (100 μg/mL) was used as a chemical negative control in both assays. DMSO, water, and BSA-water were used as vehicles for the positive controls, caffeine and particles, respectively.

Bhas 42 cells were cultured in minimum essential medium (Thermo Fisher, Massachusetts, USA), supplemented with 1 % penicillin—streptomycin (P/S; Thermo Fisher), 1 % L-glutamine (VWR; Pennsylvania, USA), and 10 % fetal bovine serum (FBS; Thermo Fisher) at 37 °C and 5 % CO_2 for four days. Then, the cells were subcultured in D5F medium (Dulbecco's modified Eagle's medium/Ham's F12 (DMEM/F12; Thermo Fisher), 5 % FBS, 1 % P/S), and incubated for three additional days before they were seeded (day 0) into 6-well plates at a density of 4×10^3 or 14×10^3 cells/well for the initiation and promotion assays, respectively. In the initiation assay, cells were treated once. The treatment was added on day 1 and removed on day 4. Then, cells were washed with phosphate-buffered saline (PBS; Gibco Life Technologies, Carlsbad, CA, USA) and fresh culture medium was added. Culture medium changes to fresh medium were performed on days 7 and 11. In the promotion assay, the cells were treated three times on days 4, 7 and 11. Then, treatments were removed on day 14, cells were washed with PBS and fresh culture medium was added. On day 21 of both assays, cells were fixed with absolute ethanol and stained with 5 % Giemsa (Sigma—Aldrich). Foci from six wells (6 replicates) per condition were counted using a Wild M3Z stereomicroscope (Wild Heerbrugg, Gais, Switzerland) with an external Leica Cold Light Source 100 (Wetzlar, Germany) following the criteria established in the OECD GD.

A concurrent cell growth assay was performed with both assays. Three wells (3 replicates) of cells were treated under the same conditions as those described for the corresponding CTA assay. On day 7, cells were trypsinized and counted after staining with trypan blue using EVE™ Counting Slides (NanoEntek, Seoul, Korea) with an EVE™ Plus Automated Cell Counter (NanoEntek). Relative cell growth was determined by comparing to that of the corresponding vehicle.

2.4. Gene expression analyses

The mRNA expression of some of the genes composing the mRNA expression profile previously described to be a predictive early cell transformation signature (Kirsch et al., 2020) was assessed after exposure of Bhas 42 cells to each of the 3D printing-derived particles. Specifically, a panel of seven mRNAs that were expected to show both increased expression (*Prl2c3* and *Il1rl1*) and decreased expression (*Postn*, *Timp4*, *Lum*, Lgals7, and *Sparcl1*) was chosen. Bhas 42 cells were treated with 6.25 μg/mL of each material following the same treatment schedule as described for the CTA (Section 2.3), both for initiation and promotion assays. On day 7, the cells were lysed using TRIzol (Thermo Fisher Scientific, Bleiswijk, Netherlands), homogenized through pipetting, and extracted with 200 μL of chloroform per mL of TRIzol reagent as recommended by the supplier. The precipitated RNA was purified using Nucleospin RNA Cleanup Assay Kit (Macherey Nagel, Hoerdt, France) following the manufacturer's instructions. RNA was eluted using 50 μL of RNase-free water, and the RNA concentrations and purities were determined via measurement of the absorbance at 260, 280 and 230 nm and calculation of the A260/A280 and A260/A230 ratios. RNAs were treated with DNase I (Thermo Fisher Scientific, Villebon-sur-Yvette,

France) and reverse-transcribed using superscript IV (Thermo Fisher Scientific, Villebon-sur-Yvette, France) following the manufacturer's instructions. Quantitative polymerase chain reaction (qPCR) analysis was performed using Takyon master mix blue dTTP noROX SYBR assay (Eurogentec, Angers, France) in a CFX96 thermocycler (Bio-Rad, Marnes-la-Coquette, France) using primer sequences and amplification conditions recommended by Kirsch et al. (2020). Actin B (*Actb*) and glyceraldehyde-3-phosphate dehydrogenase (*Gapdh*) were used as reference genes. The results were analyzed using the ΔΔCq method with REST2009 software (Pfaffl et al., 2002).

2.5. Assessment of cellular internalization

The cellular uptake of the particles was assessed via TEM imaging.

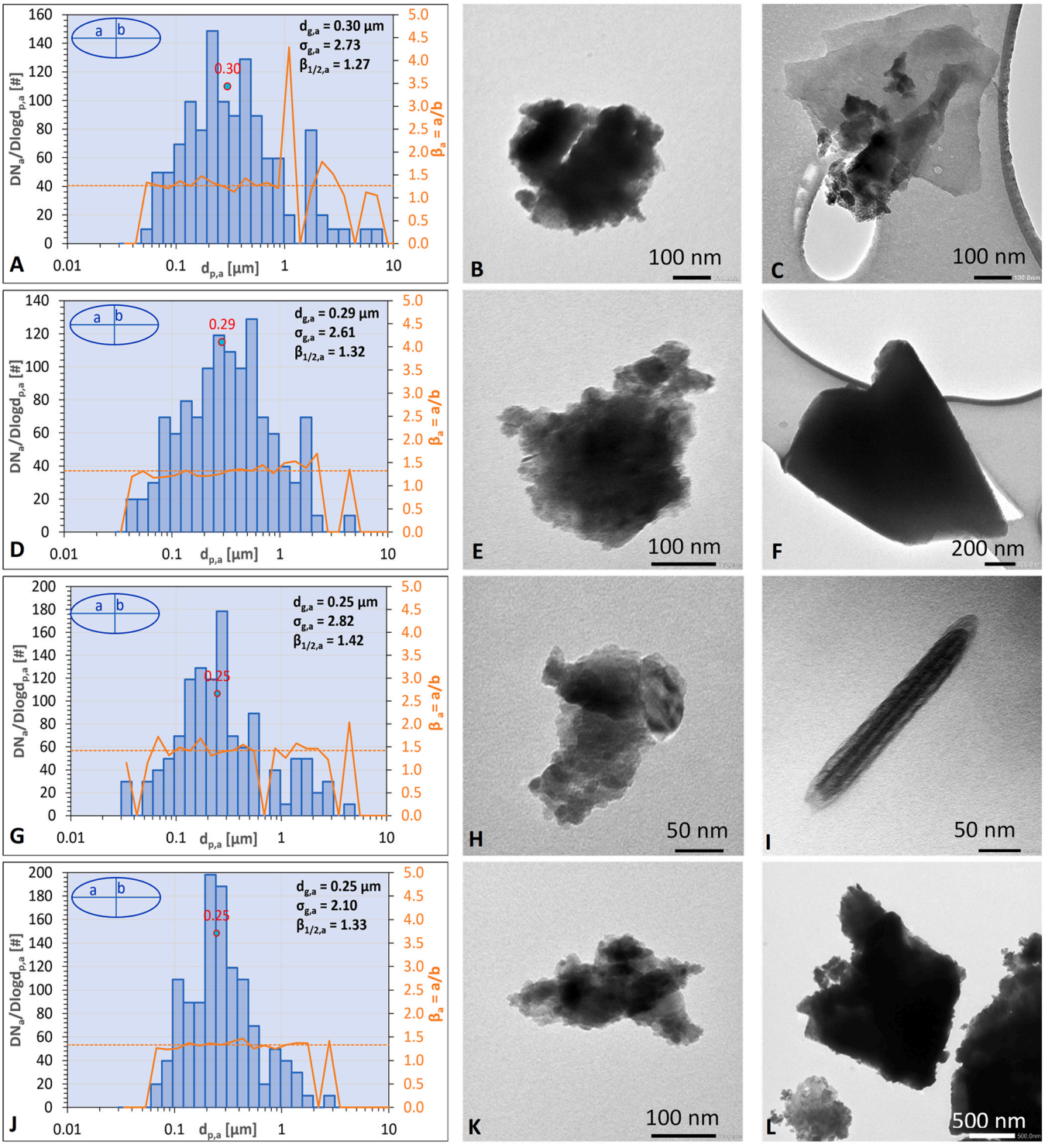

Fig. 1. Number size distribution (n = 120) of polypropylene doped with silver nanoparticles (PP-Ag; A), polypropylene (PP: D), polycarbonate doped with single-walled carbon nanotubes (PC-CNT; G), and polycarbonate (PC; J) based on the a-axis. The aspect ratio based on the a-axis (βa) is also presented. Transmission electron microscopy (TEM) images of PP-Ag (B), PP (E), PC-CNT (H), and PC (K) fragments, whose sizes are approximate to the geometric mean diameter (dg). TEM images of individual sharp-edged PP-Ag (C), PP (F), PC (L), and PC-CNT (I) fragments. The latter presents a single-walled carbon nanotube.

Bhas 42 cells were treated with 6.25 μg/mL of each material following the same treatment schedule as described for the CTA (Section 2.3), both for initiation and promotion assays. On day 7, cells were prepared for TEM imaging as described earlier (Dussert et al., 2021) and observed using a Tecnai G2 Spirit BioTwin (FEI) microscope operating at 120 K. Images were captured using an ORIUS SC1000 CCD camera (Gatan).

2.6. Statistical analyses

CTA data were statistically analyzed as recommended by the OECD (OECD, 2017) using GraphPad Prism 9.3.1 software. Focus induction was evaluated by comparison to the corresponding vehicle control via two-tailed t test for caffeine, MCA and TPA, and using one-way analysis of variance (ANOVA) with Dunett's multiple comparison test for the MNPLs. Statistical significance was set at $p \leq 0.05$.

3. Results

3.1. Characterization of the particles

The geometric mean size of most of the particles varied between 0.25 ± 2.10 and 0.30 ± 2.73 μm (Fig. 1A, D, G, J). Only a few particles (1–13 % depending on the sample) were larger than 1 μm, and practically none of them exceeded 5 μm in any of the samples.

Most of the particles were nearly spherical (Fig. 1), as also illustrated through the median aspect ratio values (1.24–1.38; Table S1). PC-based particles (Fig. 1 H, K) were slightly smaller and more elongated than PP-based particles (Fig. 1 B, E). In addition, irregular and sharp-edged particles were found in all the samples (Fig. 1C, F, L). In the case of the PC-CNT sample, some particles resembling the SWCNT morphology (approximately 40 nm in diameter and 300 nm in length) were also found (Fig. 1 I). The diameter of these fiber-like particles is bigger than the one reported for single SWCNT (1.6 nm) because they tend to form fiber-like agglomerates of several SWCNTs in the original suspension (Fig. S1). These findings were further verified using Raman spectroscopy (Fig. 2). The Raman spectrum of the PC-CNT sample (Fig. 2A) showed the characteristic SWCNT peaks (radial breathing mode, RBM, and D-, G-, and G'-bands). The G-band (1592 1/cm) and G'-band (approx. 2580 1/cm) overlapped with the characteristic PC peaks. However, the mutual relationship between the G-band and D-band (1300 1/cm), and the RBM band between 150 and 300 1/cm further confirm the presence of SWCNTs (Jorio and Saito, 2021; Shea and Wall, 2012). Neither such G- and D-band relation, nor RBM peaks were observed in the PC sample (Fig. 2B), which only showed the characteristic peaks for pristine PC. The latter were also observed in the PC-CNT sample, although at lower intensity (Fig. 2A).

For all samples, the EDX spectra (Fig. S2 and Table S2) demonstrated that the particles mainly contained C and O, as expected for plastic materials. In addition, Au, Al, Fe, Cr, and, in some cases, Cu and Si, were also found. The latter elements probably originated from the used devices, as they were detected when empty SiO-coated copper grids were analyzed (data not shown). Ag was not detected through EDX in the PP-Ag sample, likely owing to the low content of silver nanoparticles in the original filaments. However, when using ICP-MS, Ag was quantified in the PP-Ag sample at higher concentration (200.4 ppm) than that detected in the PP sample (21.77 ppm).

With regard to the hydrodynamic behavior of the particles (Table 1), minor differences in the aggregation state in both dispersants were observed for the PC-CNT and PP MNPLs, whereas for the other two materials, the average size was greater in the culture medium. No statistically significant differences in the average size among particle types or between dispersants were observed. As shown in Fig. S3, all materials with the exception of PC-CNT particles showed a spectrum within the range of 100–1000 nm when dispersed in BSA-water. The spectrum of PC-CNT covered a broader range, exceeding 1000 nm. The high PDI value of this sample may reflect the presence of large agglomerates in suspension (> 1–2 μm) that mask the DLS signal of smaller particles and distort the spectrum. Conversely, the size distribution by intensity (Fig. S3), and the average particle size and PDI (Table 1) did not show great differences among the four types of materials when dispersed in culture medium. In general, size measurements showed high variability, as expected when highly polydisperse fractions of same samples of true-to-life materials are measured using DLS (Domenech et al., 2024).

Table 1
Average particle size, polydispersity index (PDI) and surface charge (Z-potential) of polycarbonate (PC), polycarbonate doped with single-walled carbon nanotubes (PC-CNT), polypropylene (PP) and polypropylene doped with silver nanoparticles (PP-Ag) suspended in 0.05 % BSA-water and culture medium (DMEM/F12). The data are expressed as the means ± SD (n = 3).

Material	BSA-water			DMEM/F12		
	Z-average (nm)	PDI	Z-potential (mV)	Z-average (nm)	PDI	Z-potential (mV)
PC	304.0 ± 101.5	0.101	−3.76 ± 3.48	510.6 ± 324.1	0.308	−6.94 ± 1.19
PC-CNT	480.5 ± 559.0	0.766	−7.15 ± 3.42	461.9 ± 276.7	0.280	−9.35 ± 0.72
PP	399.2 ± 136.8	0.106	−11.13 ± 6.57	416.3 ± 218.5	0.225	−6.19 ± 1.57
PP-Ag	301.8 ± 191.9	0.309	−5.74 ± 6.41	430.7 ± 241.3	0.251	−9.65 ± 0.60

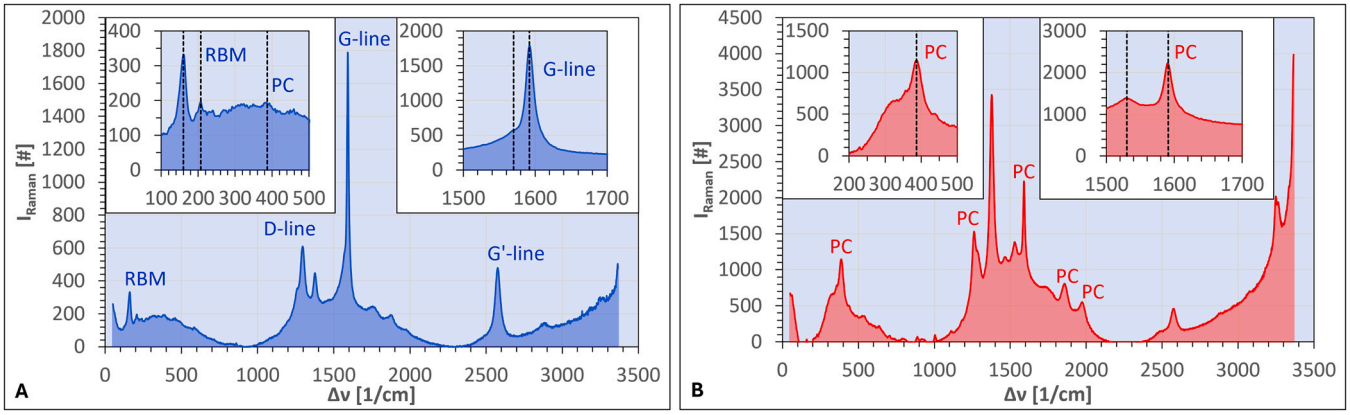

Fig. 2. Raman spectra of polycarbonate doped with single-walled carbon nanotubes (PC-CNT; A) and polycarbonate (PC; B). The characteristic Raman bands of single-walled carbon nanotubes (A; RBM, D-band, G-band, and G'-band) and polycarbonate (PC) polymer (B) are indicated in more detail in the insets. RBM= radial breathing mode.

Alternatively, all the particles had negatively charged surfaces in both dispersants without showing statistically significant differences among them, with Z-potential values varying from −3.76 to −11.13 mV, which indicates the low stability of the MNPL suspensions. It is worth mentioning that the Z-potential value of PP MNPL in BSA/water (−11.13 mV) is similar to the one reported for PP particles degraded in pure-water under UV light after 8 days of exposure (Wu et al., 2021), suggesting that the high-energy mechanical milling process used in the current study is similar to the weathering process of particles in the environment.

3.2. Cell-transforming capacity

The results of the CTA and concurrent cell growth assays are shown in Fig. 3. All the materials induced a concentration-dependent decrease in Bhas 42 cell proliferation in both the initiation and promotion assays. The effect was more pronounced under the initiation conditions, with materials showing cell growth percentages below 28 % at 25 μg/mL, whereas the corresponding percentages were above 35 % under the promotion conditions. At the highest tested concentration (100 μg/mL), PC-based particles showed approximately 25 % and 30–40 % cell growth under the initiation and promotion conditions, respectively. Conversely, at the same concentration, the PP-based materials showed approximately 1 % cell growth under the initiation conditions, but above 100 % cell growth under the promotion conditions. The latter finding should be interpreted with caution.

None of the 3D printing object-derived particles showed a significant increase in the number of transformed foci compared to those of the vehicle control, either in the initiation or in the promotion assay (Fig. 3). The three highest concentrations of all the materials under promotion conditions, as well as the two highest concentrations of PP-Ag particles under initiation conditions, could not be analyzed owing to the strong growth inhibition induced by the particles, which resulted in a lack of cell confluence at the end of the transformation assay.

3.3. Gene expression

Under the initiation conditions (Table 2, left), a significant decrease in mRNA expression was observed for almost all tested genes, except for *Postn* and *Lum* with all particles, and for *Prl2c3* in cells exposed to PC-CNT and PP-Ag particles, which did not show any significant change. The overall expression modulation factor was low, ranging from 0.60- to 0.85-fold the expression level in control cells. Conversely, in the promotion assay (Table 2, right), the mRNA expression of *Prl2c3*, *Postn* and *Lum* significantly increased by factors of ~1.8–1.9-, ~1–1.4- and ~1.5–1.7-fold, respectively, compared to that in untreated cells, while the mRNA expression of *Timp4* significantly decreased by a factor of ~0.3–0.5-fold. In addition, the expression of the other tested mRNAs, *Il1rl1*, *Lgals7* and *Sparcl1,* was not significantly modulated. These changes in mRNA expression were observed regardless of the particle polymer or doping with nanomaterials.

3.4. Internalization of particles into Bhas 42 cells

All the particles were taken up by Bhas 42 cells under both initiation (Fig. 4) and promotion (Fig. S4) conditions. Regardless of their composition, the particles could be observed in the cell cytoplasm, sometimes entrapped into vesicles (Fig. 4 and Fig. S4, arrows indicating the presence of surrounding membranes) that were not observed in untreated cells (Fig. S4A-B). However, it should be noted that visualizing a cellular membrane surrounding electron-dense materials is difficult, as the material is often tightly packed and the membrane sticks to the particle surface. For instance, a membrane entraps the particle highlighted by squares in Fig. 4B, D (left square), F (upper particle within the square) and Fig. 4H, while no membrane can be clearly distinguished around the other particles. Most of the time, vesicles showed the typical morphology of lysosomes, autophagosomes or autolysosomes (Fig. 4B and H, squares; Fig. S4D, bottom square and Fig. S4F, multiple autolysosomes in the highlighted square) previously described (Chakraborty et al., 2020). The morphology of the particles inside cells was similar to that described in Fig. 1, i.e., in acellular conditions (see insets in Fig. 4B, D, F, H). Particles showed irregular morphologies with sharp edges, and a mixture of electron-dense and electron-light materials, suggesting that some parts of the particles are thick and others are thinner, respectively. This suggests that they did not undergo any dissolution or degradation once they accumulated inside the cells. Particles were not observed in any other subcellular compartment, such as the cell nucleus, mitochondria, or endoplasmic reticulum. Both large agglomerates and/or aggregates (> 1 μm) and smaller particles could be observed (see, for instance, insets in Fig. 4D and H), suggesting that several internalization routes may be involved in cellular uptake.

4. Discussion

Most environmental MNPLs originate from the fragmentation and degradation of plastic waste, whose global world accumulation is expected to reach 3.4 billion tons by 2050 (Zhu et al., 2021). Although it is not possible to accurately estimate the contribution from 3D printing waste, the increasing use of this technique makes this exposure source relevant. An average total weekly intake of 0.01–8.7 g MNPLs has been estimated for an average 70-kg person (Domenech et al., 2024; Shi et al., 2022). However, the real concentration of MNPLs present in the human body is still unknown owing to lack of validated analytical methods (Murashov et al., 2021), and most of the *in vitro* toxicity studies use a concentration range of 3–200 μg/mL (Wright et al., 2024), similar to the one chosen in the present study. Furthermore, as recommended by the OECD GD (OECD, 2017), the chosen concentrations ranged from little or no toxicity to less than 20 % or 50 % relative cell growth under the initiation and promotion conditions, respectively. More pronounced growth inhibition was observed after 21 days of culture in the CTAs for all MNPLs than in the concurrent 7-day cell growth assays. This phenomenon has previously been reported with other substances and can be attributed to the difference in the duration of the treatment and recovery periods for each assay (Hayashi et al., 2008).

Few studies have evaluated the *in vivo* carcinogenic or *in vitro* tumorigenic capacity of MNPLs (Domenech et al., 2024) and, to the best of our knowledge, none of them have been performed with PP or PC MNPLs. Neither pristine PS nor secondary PLA nanoparticles (6.25–200 μg/mL) were able to induce cell-transforming effects in the Bhas 42 assay (Domenech et al., 2024). Conversely, secondary polyethylene terephthalate (PET) particles generated from sanding plastic bottles, which were more efficiently internalized into Bhas 42 cells than the other two materials, increased the number of transformed foci under promotion conditions. These results confirm the suitability of the Bhas 42 CTA for assessing MNPLs. In the present study, all the tested MNPLs had already been internalized into Bhas 42 cells by day 7. However, none of them showed cell-transforming effects through either a tumor initiation or a tumor promotion mode of action.

Other toxic effects, such as chronic inflammation, oxidative stress, and genotoxicity, which focus on mechanisms of carcinogens, can be used as indirect indicators of potential carcinogenicity (Domenech et al., 2023), based on the key characteristics of carcinogens (Smith, 2019). Preliminary results obtained with the Ferric Reduction Ability of Serum (FRAS) assay indicate a low potential for oxidative damage by all particles included in the present study, which did not show differences among them, independently of whether they were undoped or doped with nanomaterials (Polanco et al., manuscript in preparation). No clinical, hematological, or histopathological effects were reported in ICR mice daily treated for 4 weeks with up to 2000 mg/kg PP MPLs of two different sizes (5 μm and 10–50 μm) (Lee et al., 2023). Conversely, ICR mice intratracheally instilled with up to 5 mg/kg PP NPLs (0.66 ± 0.27 μm) five times per week for 4 weeks showed an increased inflammatory

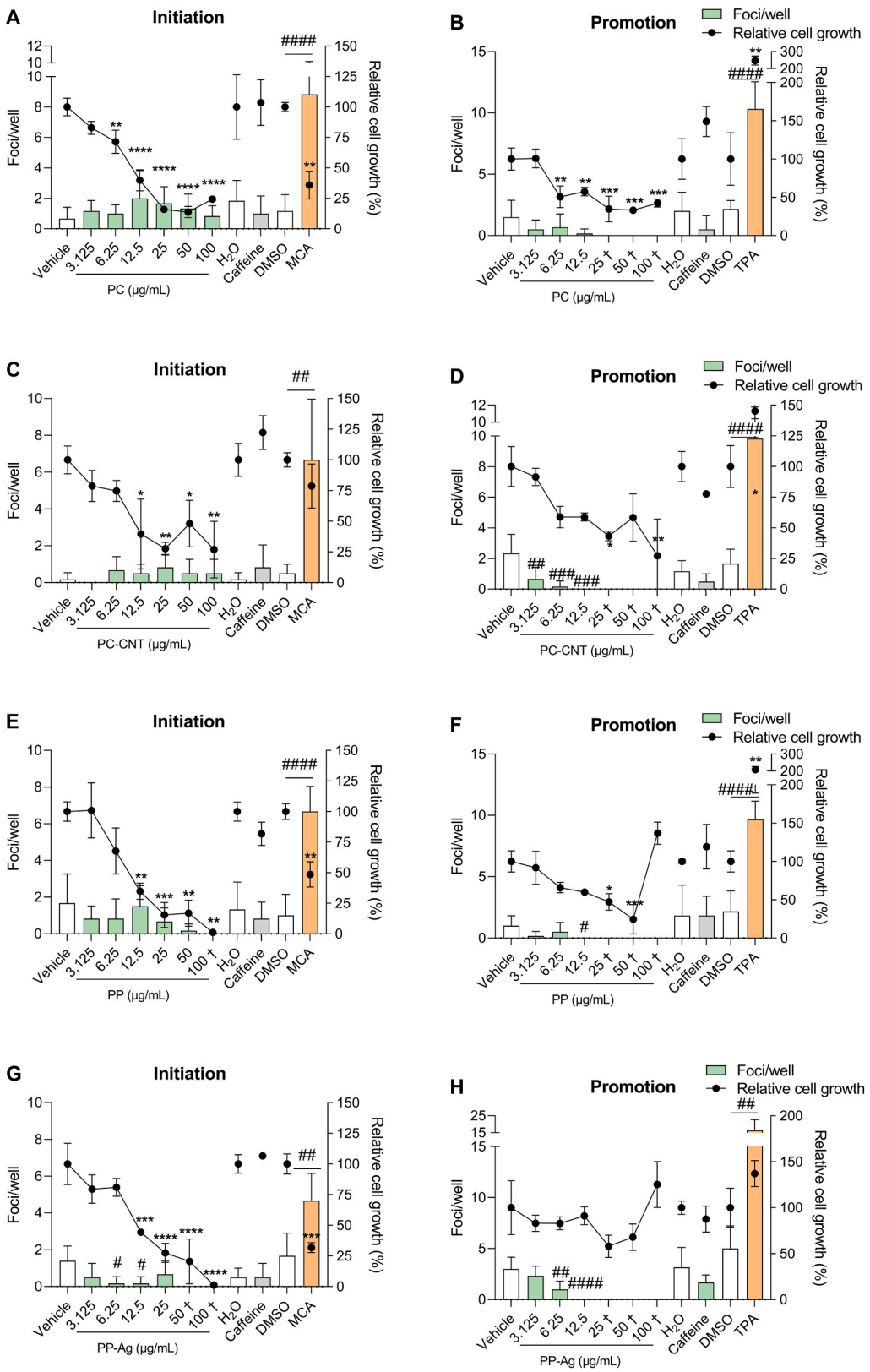

Fig. 3. Number of transformed foci per well (bars; n = 6) and percentage of relative cell growth (dots and lines; n = 3) induced by polycarbonate (PC; A and B), polycarbonate doped with single-walled carbon nanotubes (PC-CNT; C and D), polypropylene (PP; E and F) and polypropylene doped with silver nanoparticles (PP-Ag; G and H) in the Bhas 42 transformation assays. The results are expressed as the mean ± SD. 3-Methylcholanthrene (MCA) and 12-O-tetradecanoylphorbol 13-acetate (TPA), which were used as positive controls for the initiation and promotion assays, respectively, were compared with the solvent DMSO. Caffeine (negative control) was compared to water, whereas the particles were compared with the vehicle. Asterisks indicate statistical significance relative to cell growth at *$p < 0.05$, **$p < 0.01$, ***$p < 0.001$ and ****$p < 0.0001$. Hash marks indicate statistical significance relative to the number of foci/well at #$p < 0.05$, ##$p < 0.01$, ###$p < 0.001$ and ####$p < 0.0001$. The concentrations at which the cells did not reach confluence are marked with † and were excluded from foci-counting.

Table 2
mRNA expression profile of early carcinogenic biomarkers in Bhas 42 cells exposed to polycarbonate (PC), polycarbonate doped with single-walled carbon nanotubes (PC-CNT), polypropylene (PP) and polypropylene doped with silver nanoparticles (PP-Ag). The data are expressed as fold-change in gene expression (increase in bold, and decrease in italics) compared to the untreated cells ± SD (n = 4). The assessed gene expression profile comprised genes involved in cell proliferation, namely, interleukin 1 receptor like 1 (*Il1rl1*) and prolactin family 2 subfamily c3 (*Prl2c3*), as well as genes involved in cell—cell adhesion, namely, galactin 7 (*Lgals7*), periostin (*Postn*), tissue inhibitor of metalloproteinase 4 (*Timp4*), secreted protein acidic and cysteine rich like 1 (*Sparcl1*) and lumican (*Lum*).

	Initiation				**Promotion**			
	PC	**PC_CNT**	**PP**	**PP_Ag**	**PC**	**PC_CNT**	**PP**	**PP_Ag**
Il1rl1	*0.76 ± 0.04**	*0.80 ± 0.08**	*0.81 ± 0.08**	*0.85 ± 0.11**	ns	ns	ns	ns
Prl2c3	*0.83 ± 0.06**	ns	*0.74 ± 0.10**	ns	**1.88 ± 0.23***	**1.89 ± 0.29***	**1.90 ± 0.33***	**1.77 ± 0.26***
Lgals7	*0.83 ± 0.04**	*0.84 ± 0.07**	*0.81 ± 0.07**	*0.81 ± 0.09**	ns	ns	ns	ns
Postn	ns	ns	ns	ns	**1.15 ± 0.08***	**1.14 ± 0.18***	**1.22 ± 0.16***	**1.41 ± 0.15***
Timp4	*0.68 ± 0.06**	*0.60 ± 0.06**	*0.62 ± 0.08**	*0.62 ± 0.08**	*0.51 ± 0.11**	*0.35 ± 0.06**	*0.36 ± 0.05**	*0.41 ± 0.04**
Sparcl1	*0.84 ± 0.05**	*0.75 ± 0.07**	*0.67 ± 0.07**	*0.68 ± 0.09**	ns	ns	ns	ns
Lum	ns	ns	ns	ns	**1.68 ± 0.16***	**1.50 ± 0.21***	**1.56 ± 0.23***	**1.65 ± 0.21***

* Statistical significance ($p < 0.05$) obtained via a randomisation method using the REST2009 tool; ns: non-significant.

response, increased reactive oxygen species production and lung tissue damage compared to those of the vehicle group (Woo et al., 2023). Similarly, the daily administration of up to 100 mg/kg PP particles (8 and 70 μm) to C57BL/6 mice for 28 days resulted in pathological inflammatory damage, ultrastructural changes in intestinal epithelial cells, an imbalance of the redox system, and inflammatory reactions in the colon (Jia et al., 2023). On the other hand, DMSO extract of PP-based debris did not induce oxidative stress, genotoxicity or estrogenic effects in HepG2 or Caco-2 cells (Le Bihanic et al., 2025). However, information is more limited as concerns to PC MNPLs, which showed greater cytotoxicity in Caco-2 and HePG2 cells than two PET NPLs of comparable size (approx. 50 nm) (Tolardo et al., 2022). This effect may have been associated with the byproducts originated during the generation of the NPLs using laser ablation. In fact, Bisphenol A is a prevalent monomer used in the manufacture of PC plastics (Palsania et al., 2024), and it has been shown to have tumorigenic and metastatic properties in a murine breast cancer model (Torres-Alamilla et al., 2023).

Studies evaluating the toxic effects of co-exposure to MNPLs and nanomaterials are also scarce. The co-exposure to different concentrations (1–10 mg/L) of Ag (approx. 50 nm) and PS (approx. 20 nm) nanoparticles (NPs) showed additive effects on increased apoptosis and cell death, the expression of IL-6, IL-8 and TNFα, oxidative stress, and mitochondrial dysfunction in human THP-1 macrophages (Ilić et al., 2022a) and immortalized human Jurkat lymphocytes (Ilić et al., 2022b). Interestingly, all tested NP combinations significantly increased the number of double-stranded DNA breaks in THP-1 cells, which was similar to the effect of exposure to Ag NPs alone. In fact, silver nanorods (50 nm diameter, 3000 nm length), but not nanospheres (< 20 nm), induced transformed foci by a genotoxic mode of action when tested under the initiation conditions (0.1–10 μg/cm^2) of the Bhas 42 assay (Gábelová et al., 2017). Other types of silver NPs (< 100 nm) also induced a significant dose-dependent cell-transforming effect after 72-h exposure of Balb 3T3 cells to 0.17–10.60 μg/mL of particles, an approach that also recognizes tumor initiators (Choo et al., 2017). Additive or synergistic effects were not found in the present study, where the only observed difference between MNPLs undoped or doped with nanomaterials was a greater growth inhibition effect of PP-Ag than that of PP at the highest concentrations in the initiation assay. Assuming a similar concentration of silver in the PP-Ag sample as in the original filaments (0.05–0.10 wt%) and total bioavailability of silver to cells, the Bhas 42 cells of the present study would have been exposed to 0.1–0.2 μg/mL silver at the highest concentration. Although similar low concentrations of some of the silver NPs evaluated in the above-mentioned studies showed transforming effects, embedding of the silver particles into the polymeric matrix may have affected the availability of the particles to the cells. In fact, different PP nanocomposites with ultralow filling contents (0.0023–0.046 wt%) of Ag nanoplates were not cytotoxic to murine RAW264.7 macrophages nor induced cellular perturbations, as measured through nitric oxide release (Bellisario et al., 2023). However, additive/synergistic effects might be possible under real-life conditions, as shown by the increased ion-related toxicity of Ag NPs induced by PS microparticles under simulated sunlight irradiation (Tong et al., 2022), owing to the enhanced oxidative dissolution and transformation of Ag NPs induced by PS particles.

Diverse types of human cell lines have shown cancer phenotypic hallmarks (e.g., anchorage-independent cell growth, cell migration and invasion, and tumor sphere formation) after long-term exposure to several types of SWCNTs (Chatterjee and Alfaro-Moreno, 2023). However, no cell-transforming potential induced by PC MNPLs undoped or doped with SWCNTs was detected in the present study, despite some free SWCNTs were observed in the latter material. However, the release rate was probably quite low, as reported for multiwalled carbon nanotubes-enabled polymers subjected to extrusion (Stefaniak et al., 2018), weather degradation (Sahle-Demessie et al., 2023) or abrasion (Bossa et al., 2021). On the other hand, the occurrence of protruding structures of SWCNT on the surface of particles, which might make them available to cells, have previously reported during the manufacturing of the PC-CNT filaments (McLean et al., 2024). However, such structures were not observed in our analyses.

Although the *in vitro* oncotransformation detected by the Bhas 42 model closely correlates with *in vivo* tumorigenesis, this CTA model cannot cover the complexity of the *in vivo* multistage carcinogenicity process (Colacci et al., 2023). In fact, several *in vivo* (Chen et al., 2024; Kim et al., 2022; Q. Yang et al., 2023) and *in vitro* (Barguilla et al., 2022b, 2022a) studies have shown that PS MNPLs induce effects that are considered hallmarks of carcinogenesis, despite showing negative outcomes in the Bhas 42 assay (Domenech et al., 2024). The Bhas 42 assay has been suggested to be a suitable model for studying later steps in cancer progression (Colacci et al., 2023). Hence, the expression of five genes involved in cell—cell adhesion (*Lgals7*, *Lum*, *Postn*, *Sparcl1* and *Timp4*) and two genes involved in cell proliferation (*Il1rl1* and *Prl2c3*) were evaluated in the present study. These genes are part of a 12-gene signature that has previously been considered a potential early biomarker of cell transformation (Kirsch et al., 2020). The function and role of these genes in tumor onset or progression have been discussed in detail by Guichard et al. (2023), and it is summarized in Annex I (Supplementary Material). Overall decreased mRNA expression was observed in the initiation assay with all the 3D printing-derived particles, which may be related to the overall decrease in gene expression previously reported in stressed cells (Bond, 2006). Conversely, only four of the assessed genes, i.e., *Prl2c3*, *Timp4*, *Postn* and *Lum*, exhibited significant changes in expression under the promotion conditions with all the particle treatments. Our results agree with the increased and decreased *Prl2c3* and *Timp4* mRNA expression, respectively, described by Kirsch et al. (2020) under promotion conditions. However, these authors also reported decreased mRNA expression of *Postn* and *Lum*, contrary to the modulation observed here, as well as modulation of *Il1rl1*, *Lgals7* and *Sparcl1*, which was not observed in the present study.

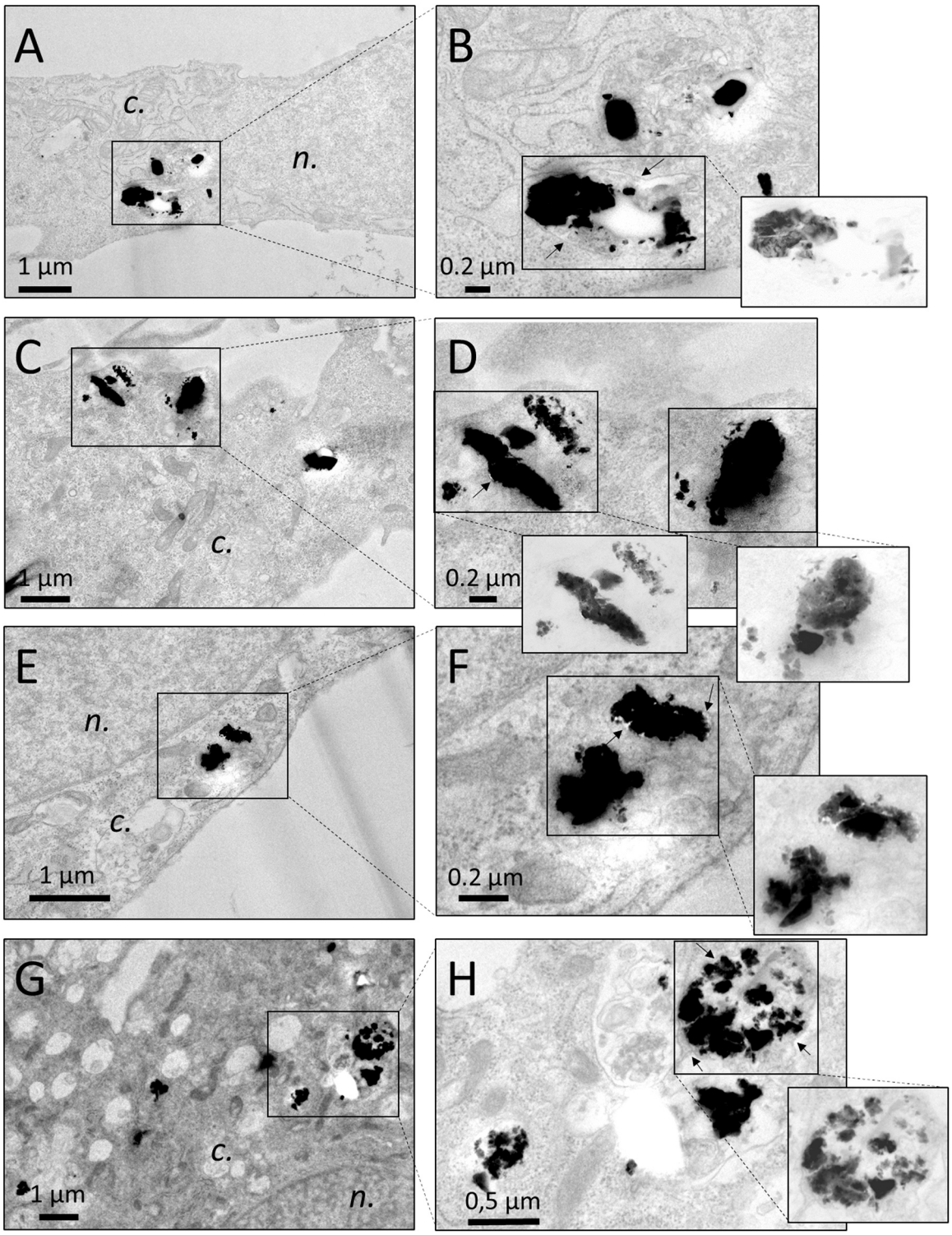

Fig. 4. Transmission electron microscopy images of Bhas 42 cells exposed to 3D printing-derived particles, in the initiation experiment: Bhas 42 cells exposed to 6.25 µg/mL polycarbonate (A, B), polycarbonate doped with single-walled carbon nanotubes (C, D), polypropylene E, F) or polypropylene doped with silver nanoparticles (G, H). B, D, F, H are higher magnification images of the region delimited by a square in A, C, E, G, respectively. Insets show images A, C, E, G with a distinct contrast, so that the structure of materials can be observed. n. nucleus, c. cytoplasm.

The incomplete mRNA expression signature observed here could be owed to the distinct mechanisms of action of the tested compounds, as reported for some substances with proven transformation capacity, or to the use of a suboptimal exposure duration (72 h) compared with the recommended one (48 h) (Guichard et al., 2023).

Notably, the significant changes in mRNA expression were observed when 3D printing-derived particles did not induce foci formation in Bhas 42 cells. Similarly, changes in the expression of *Prl2c3* and *Timp4* were also observed at low concentrations of silica nanoparticles that did not induce transformation of Bhas 42 cells (Kirsch et al., 2020). Furthermore, other cell-transforming substances, *i.e.*, TPA, mezerin and methylarsonic, also cause similar changes in the expression of both genes

(Guichard et al., 2023), suggesting that this signature could be common to a large set of substances acting via distinct mechanisms. Our results also agree with those of Park et al. (2023), who observed that 16.4 μm PP fragments of irregular shape and sharp edges obtained through cryogenic grinding of pellets (1.6 mg/mL for 12 h) did not induce morphological changes or cellular migration in human breast cancer MCF-7 and MDA-MB-231 cell lines. However, MDA-MB-231 cells treated for 24 h with PP particles showed significantly increased expression of TMBIM6, AP2M1, and PTP4A2, which are correlated with cancer progression and the cell cycle. Therefore, dysregulation of the expression of some genes, at least increased mRNA expression of *Prl2c3* and decreased expression of *Timp4*, could be a very sensitive early biomarker of cell transformation in the Bhas 42 assay, before the appearance of transformed foci.

5. Conclusions

Our findings showed that secondary MNPLs generated through cryomilling 3D-printed objects manufactured with four types of PC- and PP-modified thermoplastic filaments did not initiate or promote cell transformation in the validated *in vitro* Bhas 42 assay, regardless of polymers being doped with SWCNTs or silver nanoparticles, respectively. However, all materials induced significant dysregulation of the expression of *Prl2c3* and *Timp4* under promotion conditions, which could indicate early changes that occur before foci formation. Further studies combining *in vitro* CTAs with analyses of molecular changes are needed to accelerate the assessment of the tumorigenic potential of environmental MNPLs.

CRediT authorship contribution statement

Jesús Guzmán-Mínguez: Resources, Formal analysis. **Mikel Isasi-Vicente:** Visualization, Investigation, Formal analysis. **Alberto Katsumiti:** Supervision, Resources. **Isabel Rodríguez-Llopis**: Supervision, Funding acquisition. **Adriana Rodríguez-Garraus:** Writing – review & editing, Writing – original draft, Visualization, Investigation, Formal analysis, Data curation, Conceptualization. **Socorro Vázquez-Campos:** Supervision, Project administration, Funding acquisition. **Mari Vanäläinen:** Writing – review & editing, Visualization, Investigation, Formal analysis. **Marie Carrière:** Writing – review & editing, Writing – original draft, Visualization, Investigation, Funding acquisition, Formal analysis. **Jussi Lyyränen:** Writing – review & editing, Writing – original draft, Visualization, Investigation, Formal analysis. **Julia Catalán:** Writing – review & editing, Writing – original draft, Supervision, Project administration, Funding acquisition, Conceptualization. **Hanna Pulli:** Writing – review & editing, Visualization, Investigation, Formal analysis. **Apostolos Salmatonidis**: Writing – review & editing, Visualization, Investigation, Formal analysis. **Davide Lotti:** Resources, Funding acquisition. **Josefa Domenech:** Methodology, Conceptualization. **José F. Fernández:** Resources, Formal analysis.

Declaration of Competing Interest

The authors declare the following financial interests/personal relationships which may be considered as potential competing interests:D. L. is employee of LATI Industria Termoplastici S.p.A., Italy, the company that provided the thermoplastic filaments used in the present study. If there are other authors, they declare that they have no known competing financial interests or personal relationships that could have appeared to influence the work reported in this paper.

Acknowledgments

Arto Hurmalainen, currently working at Gammadata Finland Oy, and Petra Honkavirta, from Hosmed Oy, are greatly acknowledged for Raman analyses of the samples. This work used the electron microscopy facility at the Grenoble Structural Biology Institute, an Instruct-ERIC Centre (ISBG; UAR 3518 CNRS CEA-UGA-EMBL) with support from the French Infrastructure for Integrated Structural Biology (FRISBI; ANR-10-INSB-05–02) and GRAL, a project of the University Grenoble Alpes Graduate School (Ecoles Universitaires de Recherche) CBHEUR-GS (ANR-17-EURE-0003). The IBS electron microscope facility is supported by the Auvergne Rhône-Alpes Région, the Fonds Feder, the Fondation pour la Recherche Médicale and GIS-IBiSA.

Appendix A. Supporting information

Supplementary data associated with this article can be found in the online version at doi:10.1016/j.ecoenv.2025.118007.

Data availability

Data will be made available on request.

References

Alijagic, A., Kotlyar, O., Larsson, M., Salihovic, S., Hedbrant, A., Eriksson, U., Karlsson, P., Persson, A., Scherbak, N., Färnlund, K., Engwall, M., Särndahl, E., 2024. Immunotoxic, genotoxic, and endocrine disrupting impacts of polyamide microplastic particles and chemicals. Environ. Int. 183. https://doi.org/10.1016/J.ENVINT.2023.108412.

Azimi, P., Zhao, D., Pouzet, C., Crain, N.E., Stephens, B., 2016. Emissions of ultrafine particles and volatile organic compounds from commercially available desktop three-dimensional printers with multiple filaments. Environ. Sci. Technol. 50, 1260–1268. https://doi.org/10.1021/ACS.EST.5B04983/ASSET/IMAGES/LARGE/ES-2015-04983X_0006.JPEG.

Barguilla, I., Domenech, J., Ballesteros, S., Rubio, L., Marcos, R., Hernández, A., 2022a. Long-term exposure to nanoplastics alters molecular and functional traits related to the carcinogenic process. J. Hazard. Mater. 438, 129470. https://doi.org/10.1016/J.JHAZMAT.2022.129470.

Barguilla, I., Domenech, J., Rubio, L., Marcos, R., Hernández, A., 2022b. Nanoplastics and arsenic co-exposures exacerbate oncogenic biomarkers under an in vitro long-term exposure scenario. Int. J. Mol. Sci. 23, 2958. https://doi.org/10.3390/IJMS23062958/S1.

Bellisario, D., Santo, L., Quadrini, F., Hassiba, M., Bader, N., Chowdhury, S.H., Hassan, M.K., Zughaier, S.M., 2023. Cytotoxicity and antibiofilm activity of silver-polypropylene nanocomposites. Antibiotics 12. https://doi.org/10.3390/ANTIBIOTICS12050924.

Bond, U., 2006. Stressed out! Effects of environmental stress on mRNA metabolism. FEMS Yeast Res. 6, 160–170. https://doi.org/10.1111/J.1567-1364.2006.00032.X.

Bossa, N., Sipe, J.M., Berger, W., Scott, K., Kennedy, A., Thomas, T., Hendren, C.O., Wiesner, M.R., 2021. Quantifying mechanical abrasion of MWCNT nanocomposites used in 3D printing: influence of CNT content on abrasion products and rate of microplastic production. Environ. Sci. Technol. 55, 10332–10342. https://doi.org/10.1021/ACS.EST.0C02015/SUPPL_FILE/ES0C02015_SI_001.PDF.

Burkhardt, F., Spies, B.C., Wesemann, C., Schirmeister, C.G., Licht, E.H., Beuer, F., Steinberg, T., Pieralli, S., 2022. Cytotoxicity of polymers intended for the extrusion-based additive manufacturing of surgical guides. Sci. Rep. 12. https://doi.org/10.1038/S41598-022-11426-Y.

Chakraborty, J., Caicci, F., Roy, M., Ziviani, E., 2020. Investigating mitochondrial autophagy by routine transmission electron microscopy: Seeing is believing? Pharmacol. Res. 160, 105097. https://doi.org/10.1016/J.PHRS.2020.105097.

Champion, J.A., Walker, A., Mitragotri, S., 2008. Role of particle size in phagocytosis of polymeric microspheres. https://doi.org/10.1007/s11095-008-9562-y.

Chatterjee, N., Alfaro-Moreno, E., 2023. In vitro cell transformation assays: a valuable approach for carcinogenic potentiality assessment of nanomaterials. Int. J. Mol. Sci. 24. https://doi.org/10.3390/IJMS24098219.

Chen, G., Shan, H., Xiong, S., Zhao, Y., van Gestel, C.A.M., Qiu, H., Wang, Y., 2024. Polystyrene nanoparticle exposure accelerates ovarian cancer development in mice by altering the tumor microenvironment. Sci. Total Environ. 906, 167592. https://doi.org/10.1016/J.SCITOTENV.2023.167592.

Choo, W., Moon, B., Song, S., Oh, S.M., 2017. Morphological transformation induced by silver nanoparticles in a Balb/c 3T3 A31-1-1 mouse cell model to evaluate in vitro carcinogenic potential. Environ. Health Toxicol. 32, e2017016. https://doi.org/10.5620/EHT.E2017016.

Colacci, A., Corvi, R., Ohmori, K., Paparella, M., Serra, S., Da Rocha Carrico, I., Vasseur, P., Jacobs, M.N., 2023. The cell transformation assay: a historical assessment of current knowledge of applications in an integrated approach to testing and assessment for non-genotoxic carcinogens. Int. J. Mol. Sci. 24, 5659. https://doi.org/10.3390/IJMS24065659/S1.

Crapnell, R.D., Bernalte, E., Sigley, E., Banks, C.E., 2024. Recycled PETg embedded with graphene, multi-walled carbon nanotubes and carbon black for high-performance conductive additive manufacturing feedstock. RSC Adv. 14, 8108–8115. https://doi.org/10.1039/D3RA08524D.

Ding, W.T., Jiao, X.Y., Zhao, Y.M., Sun, X.Y., Chen, C., Wu, A.P., Ding, Y.T., Hou, P.X., Liu, C., 2023. Enhancing the electrical conductivity and strength of PET by single-

wall carbon nanotube film coating. ACS Appl. Mater. Interfaces 15, 37802–37809. https://doi.org/10.1021/ACSAMI.3C06671.
Dokuchaeva, A.A., Vladimirov, S.V., Borodin, V.P., Karpova, E.V., Vaver, A.A., Shiliaev, G.E., Chebochakov, D.S., Kuznetsov, V.A., Surovtsev, N.V., Adichtchev, S. V., Malikov, A.G., Gulov, M.A., Zhuravleva, I.Y., 2023. Influence of single-wall carbon nanotube suspension on the mechanical properties of polymeric films and electrospun scaffolds. Int. J. Mol. Sci. 24. https://doi.org/10.3390/IJMS241311092.
Domenech, J., Annangi, B., Marcos, R., Hernández, A., Catalán, J., 2023. Insights into the potential carcinogenicity of micro- and nano-plastics. Mutat. Res./Rev. Mutat. Res. 791, 108453. https://doi.org/10.1016/J.MRREV.2023.108453.
Domenech, J., Villacorta, A., Ferrer, J.F., Llorens-Chiralt, R., Marcos, R., Hernández, A., Catalán, J., 2024. In vitro cell-transforming potential of secondary polyethylene terephthalate and polylactic acid nanoplastics. J. Hazard. Mater. 469. https://doi.org/10.1016/J.JHAZMAT.2024.134030.
Dussert, F., Wegner, K.D., Moriscot, C., Gallet, B., Jouneau, P.H., Reiss, P., Carriere, M., 2021. Evaluation of the dermal toxicity of InZnP quantum dots before and after accelerated weathering: toward a safer-by-design strategy. Front. Toxicol. 3, 636976. https://doi.org/10.3389/FTOX.2021.636976/BIBTEX.
Filamentive, 2023. How much plastic waste does 3D printing really generate? [WWW Document]. URL ⟨https://www.filamentive.com/how-much-plastic-waste-does-3d-printing-really-generate/#:~:text=Aggregating%20this%20with%20the%20estimated%201%2C148%2C400%20kg%20of%20plastic%20consumption,379%2C000%20kg%20per%20year⟩. (Accessed 7.3.24).
Gábelová, A., El Yamani, N., Alonso, T.I., Buliaková, B., Srančíková, A., Bábelová, A., Pran, E.R., Fjellsbø, L.M., Elje, E., Yazdani, M., Silva, M.J., Dušinská, M., 2017. Fibrous shape underlies the mutagenic and carcinogenic potential of nanosilver while surface chemistry affects the biosafety of iron oxide nanoparticles. Mutagenesis 32, 193–202. https://doi.org/10.1093/MUTAGE/GEW045.
Global Plastics Outlook, 2022. Global Plastics Outlook. https://doi.org/10.1787/DE747AEF-EN.
Guichard, Y., Savoy, C., Gaté, L., 2023. Can a 12-gene expression signature predict the cell transforming potential of tumor promoting agents in Bhas 42 cells? Toxicol. Lett. 389, 11–18. https://doi.org/10.1016/J.TOXLET.2023.10.006.
Hayashi, K., Sasaki, K., Asada, S., Tsuchiya, T., Hayashi, M., Yoshimura, I., Tanaka, N., Umeda, M., 2008. Technical modification of the Balb/c 3T3 cell transformation assay: the use of serum-reduced medium to optimise the practicability of the protocol. Alter. Lab Anim. 36, 653–665. https://doi.org/10.1177/026119290803600609.
Hinds, W.C., 2012. Chapter 9: Filtration. Aerosol Technology: Properties, Behavior, and Measurement of Airborne Particles.
Ilić, K., Kalčec, N., Krce, L., Aviani, I., Turčić, P., Pavičić, I., Vinković Vrček, I., 2022a. Toxicity of nanomixtures to human macrophages: Joint action of silver and polystyrene nanoparticles. Chem. Biol. Interact. 368, 110225. https://doi.org/10.1016/J.CBI.2022.110225.
Ilić, K., Krce, L., Rodriguez-Ramos, J., Rico, F., Kalčec, N., Aviani, I., Turčić, P., Pavičić, I., Vinković Vrček, I., 2022b. Cytotoxicity of nanomixture: Combined action of silver and plastic nanoparticles on immortalized human lymphocytes. J. Trace Elem. Med. Biol. 73. https://doi.org/10.1016/J.JTEMB.2022.127004.
ISO 22412:2017 - Particle size analysis — Dynamic light scattering (DLS) [WWW Document], n.d. URL ⟨https://www.iso.org/standard/65410.html⟩ (Accessed 11.17.24).
ISO 24187:2023 - Principles for the analysis of microplastics present in the environment [WWW Document], n.d. URL ⟨https://www.iso.org/standard/78033.html⟩ (Accessed 11.17.24).
Jensen, K.A., Birkedal, R., Kembouche, Y., Christiansen, E., Jacobsen, N.R., Wallin, H., Guiot, C., Spalla, O., Witschger, O., 2011. "Towards a method for detecting the potential genotoxicity of nanomaterials. Deliverable 3. Final protocol for producing suitable manufactured nanomaterial exposure media. Generic Nanogenotox Dispers. Protoc. Stand. Oper. Proced. (SOP) Backgr. Doc. 1–33. ⟨https://www.anses.fr/en/system/files/nanogenotox_deliverable_6.pdf⟩ (n.d.).
Jia, R., Han, J., Liu, X., Li, K., Lai, W., Bian, L., Yan, J., Xi, Z., 2023. Exposure to Polypropylene Microplastics via Oral Ingestion Induces Colonic Apoptosis and Intestinal Barrier Damage through Oxidative Stress and Inflammation in Mice. Toxics 11. https://doi.org/10.3390/TOXICS11020127.
Jorio, A., Saito, R., 2021. Raman spectroscopy for carbon nanotube applications. J. Appl. Phys. 129, 21102. https://doi.org/10.1063/5.0030809/1025611.
Kim, H., Zaheer, J., Choi, E.J., Kim, J.S., 2022. Enhanced ASGR2 by microplastic exposure leads to resistance to therapy in gastric cancer. Theranostics 12, 3217–3236. https://doi.org/10.7150/THNO.73226.
Kirsch, A., Dubois-Pot-Schneider, H., Fontana, C., Schohn, H., Gaté, L., Guichard, Y., 2020. Predictive early gene signature during mouse Bhas 42 cell transformation induced by synthetic amorphous silica nanoparticles. Chem. Biol. Interact. 315, 108900. https://doi.org/10.1016/J.CBI.2019.108900.
LATI3Dlab, n.d. LATI3Dlab; Granules of thermoplastic compounds for 3D printing [WWW Document]. URL ⟨https://www.lati3dlab.com/en/products/plastic-granules-for-3d-printing/⟩ (Accessed 6.22.24).
Le Bihanic, F., Cormier, B., Dassié, E., Lecomte, S., Receveur, J., Le Floch, S., Cachot, J., Morin, B., 2025. Toxicity assessment of DMSO extracts of environmental aged beached plastics using human cell lines. Ecotoxicol. Environ. Saf. 289. https://doi.org/10.1016/J.ECOENV.2024.117604.
Lee, Sijoon, Kim, Dongseon, Kang, K.K., Sung, S.E., Choi, J.H., Sung, M., Shin, C.H., Jeon, E., Kim, Dongkyu, Kim, Dongmin, Lee, Sunjong, Kim, H.K., Kim, K., 2023. Toxicity and biodistribution of fragmented polypropylene microplastics in ICR mice. Int. J. Mol. Sci. 24. https://doi.org/10.3390/IJMS24108463.
Ligon, S.C., Liska, R., Stampfl, J., Gurr, M., Mülhaupt, R., 2017. Polymers for 3D printing and customized additive manufacturing. Chem. Rev. 117, 10212–10290. https://doi.org/10.1021/ACS.CHEMREV.7B00074.
McLean, P., Hanlon, J., Salmatonidis, A., Galea, K.S., Brooker, F., Citterio, C., Magni, D., Vázquez-Campos, S., Lotti, D., Boyles, M.S.P., 2024. Safe(r)-by-design principles in the thermoplastics industry: guidance on release assessment during manufacture of nano-enabled products. Front. Public Health 12, 1398104. https://doi.org/10.3389/FPUBH.2024.1398104/BIBTEX.
More, S., Bampidis, V., Benford, D., Bragard, C., Halldorsson, T., Hernández-Jerez, A., Hougaard Bennekou, S., Koutsoumanis, K., Lambré, C., Machera, K., Naegeli, H., Nielsen, S., Schlatter, J., Schrenk, D., Silano, V., Turck, D., Younes, M., Castenmiller, J., Chaudhry, Q., Cubadda, F., Franz, R., Gott, D., Mast, J., Mortensen, A., Oomen, A.G., Weigel, S., Barthelemy, E., Rincon, A., Tarazona, J., Schoonjans, R., 2021. Guidance on risk assessment of nanomaterials to be applied in the food and feed chain: human and animal health. EFSA J. 19. https://doi.org/10.2903/J.EFSA.2021.6768.
Murashov, V., Geraci, C.L., Schulte, P.A., Howard, J., 2021. Nano- and microplastics in the workplace. J. Occup. Environ. Hyg. 18, 489. https://doi.org/10.1080/15459624.2021.1976413.
NIOSH, 2020. 3D Printing with Filaments: Health and Safety Questions to Ask. https://doi.org/10.26616/NIOSHPUB2020115.
OECD. Guidance Document on the in Vitro Bhas 42 Cell Transformation Assay. Series on Testing & Assessment No. 231, 2017. Organisation for Economic Co-operation and Development.
Palsania, P., Singhal, K., Dar, M.A., Kaushik, G., 2024. Food grade plastics and Bisphenol A: associated risks, toxicity, and bioremediation approaches. J. Hazard Mater. 466. https://doi.org/10.1016/J.JHAZMAT.2024.133474.
Park, J.H., Hong, Seungwoo, Kim, O.H., Kim, C.H., Kim, J., Kim, J.W., Hong, Sungguan, Lee, H.J., 2023. Polypropylene microplastics promote metastatic features in human breast cancer. Sci. Rep. 13. https://doi.org/10.1038/S41598-023-33393-8.
Patti, A., 2024. Challenges to improve extrusion-based additive manufacturing process of thermoplastics toward sustainable development. Macromol. Rapid Commun. https://doi.org/10.1002/MARC.202400249.
Peng, M., Grootaert, C., Vercauteren, M., Boon, N., Janssen, C., Rajkovic, A., Asselman, J., 2024. Probing long-term impacts: low-dose polystyrene nanoplastics exacerbate mitochondrial health and evoke secondary glycolysis via repeated and single dosing. Environ. Sci. Technol. 58, 9967–9979. https://doi.org/10.1021/ACS.EST.3C10868/SUPPL_FILE/ES3C10868_SI_001.PDF.
Pfaffl, M.W., Horgan, G.W., Dempfle, L., 2002. Relative expression software tool (REST©) for group-wise comparison and statistical analysis of relative expression results in real-time PCR. Nucleic Acids Res. 30, e36. https://doi.org/10.1093/NAR/30.9.E36.
Pfohl, P., Wagner, M., Meyer, L., Domercq, P., Praetorius, A., Hüffer, T., Hofmann, T., Wohlleben, W., 2022. Environmental degradation of microplastics: how to measure fragmentation rates to secondary micro- and nanoplastic fragments and dissociation into dissolved organics. Environ. Sci. Technol. 56, 11323–11334. https://doi.org/10.1021/ACS.EST.2C01228/ASSET/IMAGES/LARGE/ES2C01228_0009.JPEG.
Plastic Pollution - Our World in Data [WWW Document], 2023. URL https://ourworldindata.org/plastic-pollution (Accessed 10.23.24).
Plastics Europe, 2023. Plastic- the fast facts 2023 [WWW Document]. URL https://plasticseurope.org/wp-content/uploads/2023/10/Plasticsthefastfacts2023-1.pdf (Accessed 6.22.24).
Prata, J.C., 2018. Airborne microplastics: Consequences to human health? Environ. Pollut. 234, 115–126. https://doi.org/10.1016/J.ENVPOL.2017.11.043.
Sahle-Demessie, E., Han, C., Varughese, E., Acrey, B., Zepp, R., 2023. Fragmentation and release of pristine and functionalized carbon nanotubes from epoxy-nanocomposites during accelerated weathering. Environ. Sci. Nano 10, 1812. https://doi.org/10.1039/D2EN01014C.
Shea, M.J., Wall, M.H., 2012. Representative Raman measurements of carbon nanotubes 24. https://doi.org/10.1016/j.physrep.2004.10.006.
Shi, X., Wang, X., Huang, R., Tang, C., Hu, C., Ning, P., Wang, F., 2022. Cytotoxicity and genotoxicity of polystyrene micro- and nanoplastics with different size and surface modification in A549 Cells. Int. J. Nanomed. 17, 4509–4523. https://doi.org/10.2147/IJN.S381776.
Sipe, J.M., Bossa, N., Berger, W., von Windheim, N., Gall, K., Wiesner, M.R., 2022. From bottle to microplastics: Can we estimate how our plastic products are breaking down? Sci. Total Environ. 814. https://doi.org/10.1016/J.SCITOTENV.2021.152460.
Smith, M.T., 2019. Key characteristics of carcinogens. Tumour Site Concord. Mech. Carcinog.
Sola, A., Trinchi, A., 2023. Recycling as a key enabler for sustainable additive manufacturing of polymer composites: a critical perspective on fused filament fabrication. Polymers 15. https://doi.org/10.3390/POLYM15214219.
Stefaniak, A.B., Bowers, L.N., Cottrell, G., Erdem, E., Knepp, A.K., Martin, S.B., Pretty, J., Duling, M.G., Arnold, E.D., Wilson, Z., Krider, B., Fortner, A.R., LeBouf, R.F., Virji, M.A., Sirinterlikci, A., 2022. Towards sustainable additive manufacturing: the need for awareness of particle and vapor releases during polymer recycling, making filament, and fused filament fabrication 3-D printing. Resour. Conserv. Recycl. 176. https://doi.org/10.1016/J.RESCONREC.2021.105911.
Stefaniak, A.B., Bowers, L.N., Knepp, A.K., Virji, M.A., Birch, E.M., Ham, J.E., Wells, J.R., Qi, C., Schwegler-Berry, D., Friend, S., Johnson, A.R., Martin, S.B., Qian, Y., LeBouf, R.F., Birch, Q., Hammond, D., 2018. Three-dimensional printing with nano-enabled filaments releases polymer particles containing carbon nanotubes into air. Indoor Air 28, 840–851. https://doi.org/10.1111/INA.12499.
Stefaniak, A.B., Johnson, A.R., du Preez, S., Hammond, D.R., Wells, J.R., Ham, J.E., LeBouf, R.F., Martin, S.B., Duling, M.G., Bowers, L.N., Knepp, A.K., de Beer, D.J., du

Plessis, J.L., 2019. Insights into emissions and exposures from use of industrial-scale additive manufacturing machines. Saf. Health Work 10, 229–236. https://doi.org/10.1016/J.SHAW.2018.10.003.

Tolardo, V., Magrì, D., Fumagalli, F., Cassano, D., Athanassiou, A., Fragouli, D., Gioria, S., 2022. In vitro high-throughput toxicological assessment of nanoplastics. Nanomaterials 12. https://doi.org/10.3390/NANO12121947.

Tong, L., Duan, P., Tian, X., Huang, J., Ji, J., Chen, Z., Yang, J., Yu, H., Zhang, W., 2022. Polystyrene microplastics sunlight-induce oxidative dissolution, chemical transformation and toxicity enhancement of silver nanoparticles. Sci. Total Environ. 827. https://doi.org/10.1016/J.SCITOTENV.2022.154180.

Torres-Alamilla, P., Castillo-Sanchez, R., Cortes-Reynosa, P., Gomez, R., Perez Salazar, E., 2023. Bisphenol A increases the size of primary mammary tumors and promotes metastasis in a murine model of breast cancer. Mol. Cell Endocrinol. 575. https://doi.org/10.1016/J.MCE.2023.111998.

Tse, I., Jay, A., Na, I., Murphy, S., Niño-Martínez, N., Martínez-Castañon, G.A., Magrill, J., Bach, H., 2021. Antimicrobial activity of 3D-printed acrylonitrile butadiene styrene (ABS) polymer-coated with silver nanoparticles. Materials 14. https://doi.org/10.3390/MA14247681.

Woo, J.H., Seo, H.J., Lee, J.Y., Lee, I., Jeon, K., Kim, B., Lee, K., 2023. Polypropylene nanoplastic exposure leads to lung inflammation through p38-mediated NF-κB pathway due to mitochondrial damage. Part Fibre Toxicol. 20. https://doi.org/10.1186/S12989-022-00512-8.

Wright, S., Cassee, F.R., Erdely, A., Campen, M.J., 2024. Micro- and nanoplastics concepts for particle and fibre toxicologists. Part Fibre Toxicol. 21. https://doi.org/10.1186/S12989-024-00581-X.

Wu, X., Liu, P., Gong, Z., Wang, H., Huang, H., Shi, Y., Zhao, X., Gao, S., 2021. Humic acid and fulvic acid hinder long-term weathering of microplastics in lake water. Environ. Sci. Technol. 55, 15810–15820. https://doi.org/10.1021/ACS.EST.1C04501/SUPPL_FILE/ES1C04501_SI_001.PDF.

Yang, Q., Dai, H., Wang, B., Xu, J., Zhang, Y., Chen, Y., Ma, Q., Xu, F., Cheng, H., Sun, D., Wang, C., 2023. Nanoplastics shape adaptive anticancer immunity in the colon in mice. Nano Lett. 23, 3516–3523. https://doi.org/10.1021/ACS.NANOLETT.3C00644/SUPPL_FILE/NL3C00644_SI_001.PDF.

Yang, T., Gao, M., Nowack, B., 2023. Formation of microplastic fibers and fibrils during abrasion of a representative set of 12 polyester textiles. Sci. Total Environ. 862, 160758. https://doi.org/10.1016/J.SCITOTENV.2022.160758.

Zhang, Z., Gao, X., 2022. Polypropylene random copolymer based composite used for fused filament fabrication: printability and properties. Polymers 14. https://doi.org/10.3390/POLYM14061106.

Zhao, X., You, F., 2024. Microplastic human dietary uptake from 1990 to 2018 grew across 109 major developing and industrialized countries but can be halved by plastic debris removal. Environ. Sci. Technol. 58, 8709–8723. https://doi.org/10.1021/ACS.EST.4C00010/SUPPL_FILE/ES4C00010_SI_002.XLSX.

Zhu, C., Li, T., Mohideen, M.M., Hu, P., Gupta, R., Ramakrishna, S., Liu, Y., 2021. Realization of circular economy of 3D printed plastics: a review. Polymers 13, 744. https://doi.org/10.3390/POLYM13050744.